

Finite-Reynolds-number effects in turbulence using logarithmic expansions

By K. R. SREENIVASAN¹ AND A. BERSHADSKII²

¹The Abdus Salam International Centre for Theoretical Physics, 34014 Trieste, Italy

²ICAR, P.O. Box 31155, Jerusalem 91000, Israel

(Received 4 August 2005 and in revised form 14 January 2006)

Experimental or numerical data in turbulence are invariably obtained at finite Reynolds numbers whereas theories of turbulence correspond to infinitely large Reynolds numbers. A proper merger of the two approaches is possible only if corrections for finite Reynolds numbers can be quantified. This paper heuristically considers examples in two classes of finite-Reynolds-number effects. Expansions in terms of logarithms of appropriate variables are shown to yield results in agreement with experimental and numerical data in the following instances: the third-order structure function in isotropic turbulence, the mixed-order structure function for the passive scalar and the Reynolds shear stress around its maximum point. Results suggestive of expansions in terms of the inverse logarithm of the Reynolds number, also motivated by experimental data, concern the tendency for turbulent structures to cluster along a line of observation and (more speculatively) for the longitudinal velocity derivative to become singular at some finite Reynolds number. We suggest an elementary hydrodynamical process that may provide a physical basis for the expansions considered here, but note that the formal justification remains tantalizingly unclear.

1. Introduction

If there is a unique state of turbulence at infinitely high Reynolds number, the question arises as to how to discern its properties from experiments and simulations at finite Reynolds numbers. The successful history of critical phenomena can be thought to be due to a powerful interplay between experiments on the one hand and, on the other hand, theories that accounted for the ‘finite’ effects (such as due to finite size and finite ‘distances’ away from the critical point). In turbulence, we should admit to knowing no formal way of inferring the right expansions around the infinite-Reynolds-number state, but offer here a few suggestive examples where logarithmic or inverse logarithmic expansions can be given reasonable justification and seem to play a constructive role – in so far as they allow us to obtain some new results and organize existing data more systematically. Logarithmic expansions do arise in field theory, and their appropriateness can be established there by partial resummations but these tools do not work for turbulence. The only past instances where inverse logarithmic expansions were employed in turbulence seem to be those in Barenblatt (1993), Barenblatt & Goldenfeld (1995), Barenblatt, Chorin & Prostokishin (1997), Castaing, Gagne & Hopfinger (1990) and Dubrulle (1996). We shall not duplicate the examples that these authors have ably discussed, but examine other instances after introducing each of them briefly in the following sections.

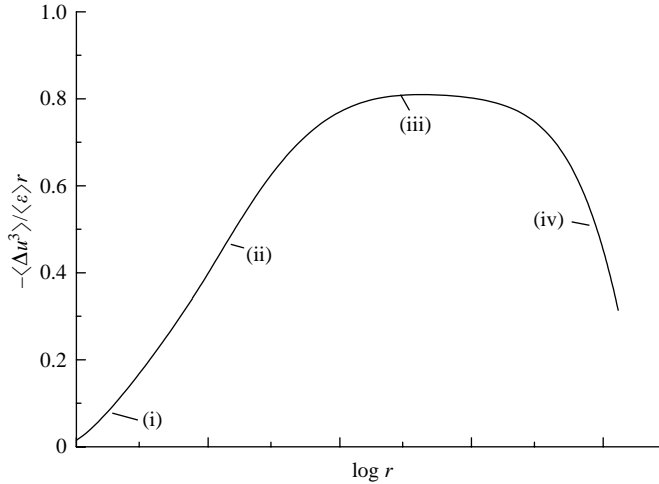


FIGURE 1. A qualitative sketch of the Kolmogorov function $-\langle \Delta u_r^3 \rangle / \langle \varepsilon \rangle r$, in terms of the scale separation r .

The next two sections deal with logarithmic expansions: §2 considers the Kolmogorov and Yaglom laws in isotropic turbulence, while §3 considers wall-bounded flows. Sections 4 and 5 consider respectively inverse logarithmic expansions for the clustering exponents of turbulent structures along an axis of intersection, and for the flatness factor of velocity derivatives. In each case, results of these expansions are compared with data from experiments and direct numerical simulations (DNS). Section 6 discusses physical mechanisms in possible support of log-expansions in turbulence.

2. Results for the inertial range of isotropic turbulence

We restrict attention to stationary isotropic turbulence without concerning ourselves with the effects of shear, though we expect the results to hold for shear flows as well.

2.1. The Kolmogorov law in isotropic turbulence

The intermediate scales between the large scale L and the dissipation (or Kolmogorov) scale η is called the inertial range. The inertial range of scales is associated with the 4/5ths law of Kolmogorov (1941) which states that

$$\langle \Delta u_r^3 \rangle = -\frac{4}{5} \langle \varepsilon \rangle r. \quad (2.1)$$

Here, $\Delta u_r \equiv u(x+r) - u(x)$ is the longitudinal velocity increment, u is the velocity component in the direction x , and $\langle \varepsilon \rangle$ is the average of the energy dissipation rate, ε . The Kolmogorov law has a special status in turbulence as it is exact – since it is derived from the Navier–Stokes equations subject only to the asymptotic requirement of ‘sufficiently high’ Reynolds number.

The qualitative behaviour of $\langle \Delta u_r^3 \rangle$, called the third-order structure function, across the entire range of scales is shown in figure 1. The part labelled (i) is obtained by a Taylor expansion in the limit of $r \rightarrow 0$, and that labelled (iii) corresponds to the region of constant energy flux where the Kolmogorov law is valid. Part (iv) depends on the properties of large scales of the flow. Very little is known about the form of the part labelled (ii), although there exists an interpolation formula for the corresponding

region in even moments (Batchelor 1951; Stolovitzky, Sreenivasan & Juneja 1993). The part (iii) corresponding to (2.1) is expected to appear at high Reynolds numbers and become more extensive with increasing Reynolds number. Experimentally, there are claims that part (iii) appears even at modest Reynolds numbers but that its enlargement is very slow in Reynolds number – certainly slower than the growth of the ratio between integral and Kolmogorov scales.

To analyse the behaviour at finite Reynolds numbers, consider the Navier–Stokes equations for a viscous incompressible fluid with random force $\mathbf{f}(\mathbf{x}, t)$, given by

$$\frac{\partial u_i}{\partial t} + u_j \frac{\partial u_i}{\partial x_j} = -\frac{1}{\rho} \frac{\partial p}{\partial x_i} + \nu \frac{\partial^2 u_i}{\partial x_j^2} + f_i(\mathbf{x}, t), \tag{2.2a}$$

$$\frac{\partial u_i}{\partial x_i} = 0, \tag{2.2b}$$

where ν is kinematic viscosity and ρ is the fluid density. Since the potential part of the external force can be included in the pressure gradient, the force can be assumed to be solenoidal. To simplify considerations below, \mathbf{f} will be assumed to be Gaussian with zero mean and a rapidly oscillating character, or a δ -correlation in time (Kraichnan 1968). Such fields are defined completely by their second-rank correlation tensor

$$\langle f_i(\mathbf{x} + \mathbf{r}, t + \tau) f_j(\mathbf{x}, t) \rangle F_{ij}(\mathbf{r}) \delta(\tau). \tag{2.3}$$

Novikov (1965) used (2.2) and (2.3) to show that the second- and third-order longitudinal structure functions are related by the equation

$$S_3 = 6\nu \frac{dS_2}{dr} - \frac{2}{r^4} \int_0^r x^4 F_{ii}(x) dx, \tag{2.4}$$

where $S_n \equiv \langle \Delta u^n \rangle$. Novikov also showed that

$$F_{ii}(0) = 2\langle \varepsilon \rangle. \tag{2.5}$$

Thus, F_{ii} corresponds to an external energy input rate, an assertion that is also supported by Novikov’s relation $\langle f_i(\mathbf{x}, t) v_j(\mathbf{x}', t) \rangle = \frac{1}{2} F_{ij}(\mathbf{x} - \mathbf{x}')$.

For $r \ll L$, it can be shown readily from (2.4) and (2.5) (see Novikov 1965) that

$$S_3 \simeq 6\nu \frac{dS_2}{dr} - \frac{4}{5} \langle \varepsilon \rangle r. \tag{2.6}$$

Without the viscous term, this is indeed Kolmogorov’s 4/5ths law. Kolmogorov obtained the result without assumptions on the nature of forcing, but our point is that the formalism, which we use below, is consistent with the exact result.

Let us rewrite (2.4) formally as

$$S_3 = -\frac{2}{r^4} \int_0^r x^4 \tilde{F}(x) dx, \tag{2.7}$$

where we define the generalized energy input rate as

$$\tilde{F}(x) \equiv F_{ii}(x) - \frac{3\nu}{x^4} \frac{d(x^4 dS_2/dx)}{dx}. \tag{2.8}$$

Assuming the existence of a local maximum of the generalized energy input rate, i.e. a local maximum of $\tilde{F}(x)$ at $x = x_m$ (where $\eta < x_m < L$), let us expand it in terms of the logarithm of the relative distance from x_m :

$$\tilde{F}(x) = \tilde{F}(x_m) - a_1 (\ln(x/x_m))^2 + \dots + a_{n-1} (\ln(x/x_m))^{n-1} + \dots, \tag{2.9}$$

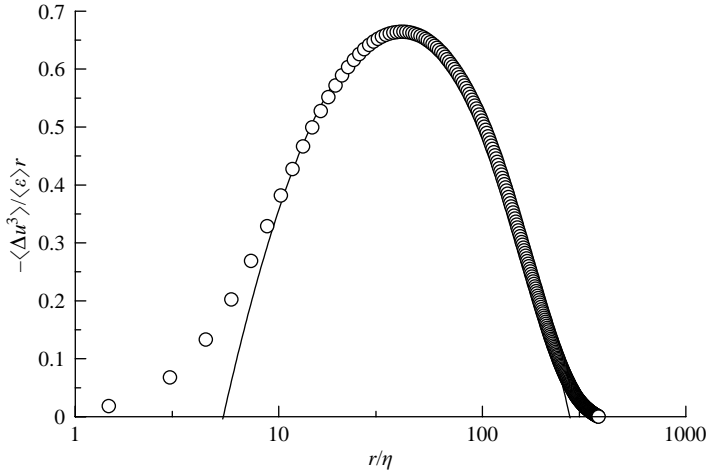


FIGURE 2. Normalized third-order structure function $-\Delta u_r^3/\langle\varepsilon\rangle r$ against $\log(r/\eta)$. The DNS data are from Gotoh *et al.* (2002), $R_\lambda = 125$. The solid parabola corresponds to (2.12).

with $a_1 > 0$. The novelty, even if it is obvious in hindsight, is the expansion in terms of $\ln x$ instead of x . This seems reasonable because the scale-to-scale energy transfer in turbulence is presumed to occur in logarithmically equal intervals.

Retaining only the two first terms in the expansion (2.9):

$$\tilde{F}(x) \simeq \tilde{F}(x_m) - a_1(\ln(x/x_m))^2, \quad (2.10)$$

we may rewrite (2.10) from dimensional considerations (see (2.5)) as

$$\tilde{F}(x) \simeq 2\langle\varepsilon\rangle A[1 - B(\ln(x/x_m))^2], \quad (2.11)$$

where A and B are dimensionless constants. This form also emphasizes the physical nature of \tilde{F} as a generalized energy input rate. Substituting (2.11) into (2.7) we obtain

$$\langle\Delta u_r^3\rangle \simeq -\frac{4}{5}\langle\varepsilon\rangle r C[1 - D \ln(r/r_m)]^2, \quad (2.12)$$

where the constants $C = A/(1 - B/2)$, $D = B/(1 - B/2)$, $r_m \simeq 1.22x_m$. Comparing (2.12) with the Kolmogorov law (2.1), it is appropriate to name $r = r_m$ the *inertial* point. Equation (2.12) is the finite-Reynolds-number form of the third-order structure function.

Figure 2 shows $-\langle\Delta u_r^3\rangle/\langle\varepsilon\rangle r$ against $\log(r/\eta)$ from the high-resolution DNS data of Gotoh, Fukayama & Nakano (2002) for homogeneous, isotropic and steady three-dimensional turbulence. The microscale Reynolds number $R_\lambda = 125$. A parabola indicates the applicability of (2.12). Figure 3 shows a similar plot for $R_\lambda = 460$ (triangles) and for the wind tunnel data of Pearson, Krogstad & van de Water (2002), obtained behind a grid for a close value of $R_\lambda = 487$. The parabola again shows (2.12).

Figures 2 and 3 demonstrate that (2.12) is a good approximation for the main part of S_3 at small and moderately high Reynolds numbers. The constant C approaches unity from below as R_λ increases, consistent with the Kolmogorov law; see figure 4 (the data point added from a high-Reynolds-number atmospheric boundary layer will be discussed below). The 4/5ths region is barely discernible for $R_\lambda \approx 500$ in some flows, though this is not true for all of them. The R_λ -variations of the inertial point r_m (i.e. x_m) and the constant D are shown in figures 5 and 6. These two variations are

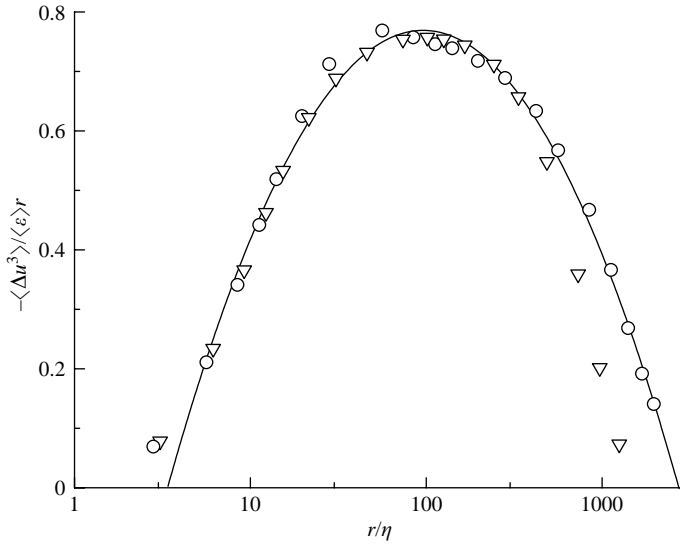


FIGURE 3. As in figure 2 but for $R_\lambda = 460$ (triangles) and for the wind-tunnel experiment of Pearson *et al.* (2002) at a close value of $R_\lambda = 487$ (circles).

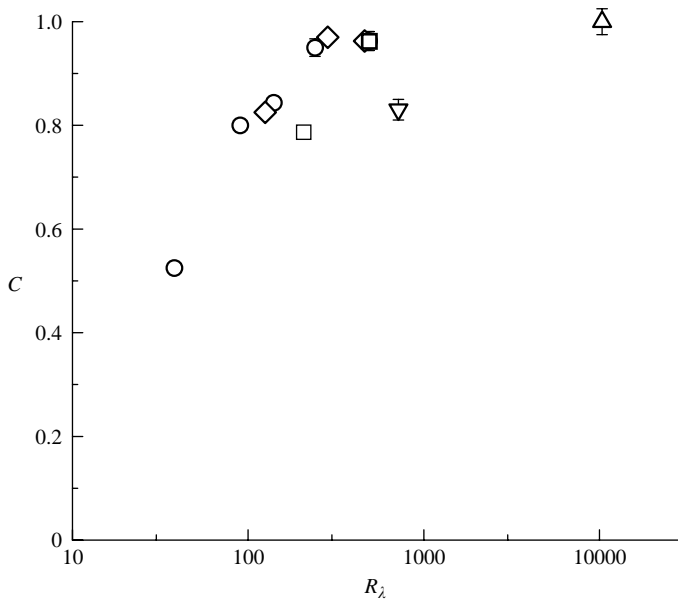


FIGURE 4. Dependence of the dimensionless constant C in (2.12) on R_λ . Symbols: circles, DNS of Donzis, Sreenivasan & Yeung (2005); diamonds, DNS of Gotoh *et al.* (2002); squares, wind-tunnel measurements of Pearson *et al.* (2002); inverted triangles, measurements behind an active grid of Kang, Chester & Meneveau (2003); upright triangles, measurements of Sreenivasan & Dhruva (1998) in the atmospheric surface layer.

not independent. Indeed, one can calculate the second derivative of the generalized energy input rate $\tilde{F}(x)$ at its maximum point x_m , and estimate D in (2.12) as

$$D \sim (r_m/\eta)^{-4/3} \sim R_\lambda^{-0.97}. \tag{2.13}$$

This estimate is close to the scaling observed in figure 5.

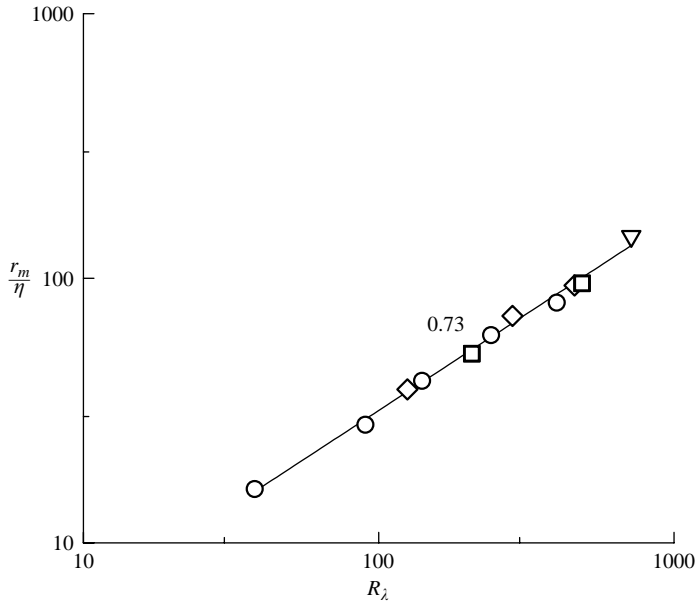


FIGURE 5. Dependence of the normalized scale r_m/η on R_λ in log-log scales. The best linear fit indicates the scaling relation $r_m/\eta \sim R_\lambda^{0.73 \pm 0.05}$. Symbols have the same meaning as in figure 4.

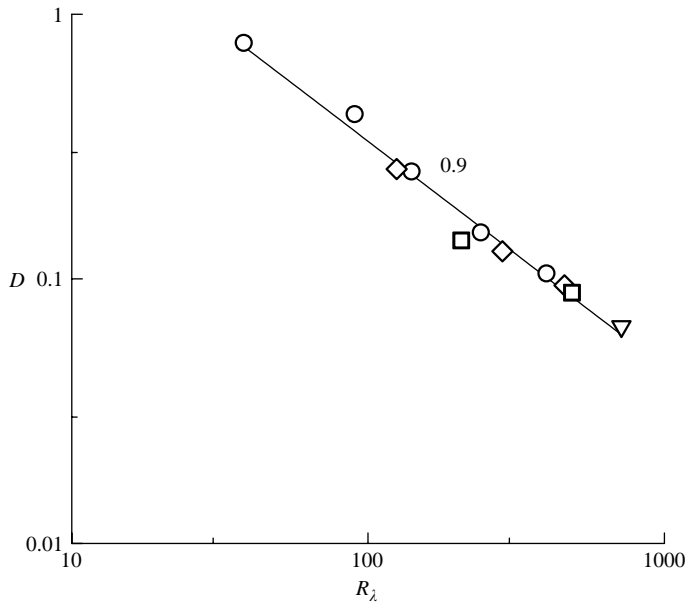


FIGURE 6. Dependence of the dimensionless constant D on R_λ in log-log scales. The best linear fit indicates the scaling relation $D \sim R_\lambda^{-0.9 \pm 0.1}$. Symbols have the same meaning as in figure 4.

What occurs at even higher Reynolds numbers is unclear because no data are available in isotropic turbulence at substantially higher R_λ . The highest-Reynolds-number data available today are from the simulations of Kaneda *et al.* (2003) but, for them, the third-order structure function has not been calculated. In any case, since

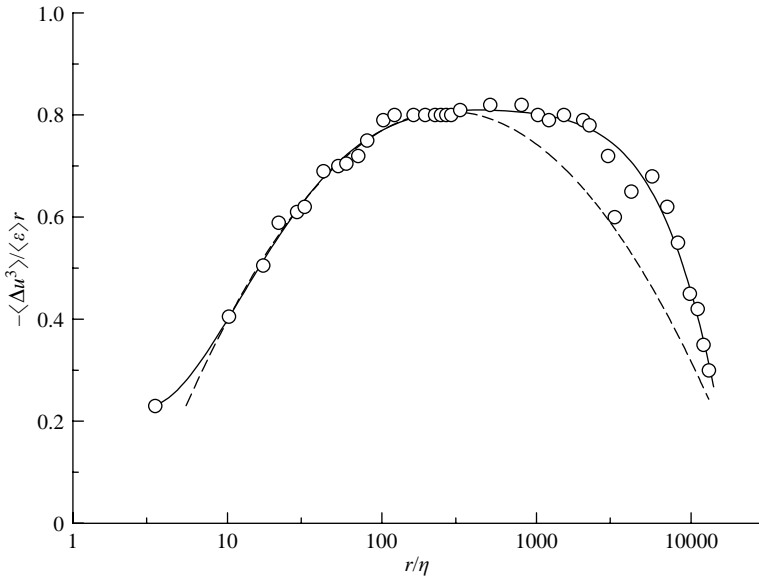


FIGURE 7. As in figure 2 but for an atmospheric experiment (Sreenivasan & Dhruva 1998) at $R_\lambda = 10400$. The solid curve corresponds to the expansion (2.9) up to the sixth order. The dashed parabola is (2.12) (i.e. (2.9) with just two terms in the expansion).

those data were run for only two turnover times of the large scale, it is unclear if S_3 has become independent of initial conditions. Thus, the transition from (2.12) to the Kolmogorov law $S_3 \equiv -\frac{4}{5}\langle\epsilon\rangle r$ can be discussed only by using data from shear flows. This discussion will be somewhat speculative because the inevitably present anisotropy may play some role (see, for example, the jet data of Gagne *et al.* 2004).

Figure 7 shows the data for atmospheric turbulence at $R_\lambda = 10\,340$ (see Sreenivasan & Dhruva (1998) for a description of the measurements). The dashed parabola, representing (2.12), is a good fit to region (ii) and some part of (iii) of figure 1. (It is from this fit that we obtained C shown in figure 3.) The solid curve, corresponding to the approximation (2.9) up to the sixth order, fits the entire curve.

There are two possible interpretations. One is that, beyond a certain R_λ , the inertial point ceases to vary with R_λ , the log terms vanish identically, and the classical inertial range is recovered (Tabeling & Willaime 2002). The main change that would occur beyond such a limiting Reynolds number is that the flat region (iii) increases in extent and accumulates to the right of r_m . In this scenario, only the region (ii) of figure 1, up to and perhaps just beyond r_m , would be fitted by (2.12). If so, the left edge of the inertial range would correspond to $r < r_m$ (or x_m), and the generalized energy input rate $\tilde{F}(x) = \tilde{F}(x_m) = \text{const}$ to the right of x_m . Alternatively, the good agreement with the high-order expansion may suggest that the log expansion with additional terms is valid even at very high Reynolds numbers, and the classical inertial range is attained at much higher Reynolds numbers than ever considered before.

2.2. The Yaglom law for passive scalars

The equivalent of Kolmogorov’s law for passive scalars is due to Yaglom (Monin & Yaglom 1975) and states that the mixed third-order structure function is given by

$$\langle \Delta u_r \Delta \theta_r^2 \rangle = -\frac{4}{3} \langle \chi \rangle r, \tag{2.14}$$

where $\Delta\theta_r \equiv \theta(x+r) - \theta(x)$ is the increment of the passive scalar θ over a scale of size r and $\langle \chi \rangle$ is the average value of the dissipation rate of scalar variance, χ . This formula is valid in the so-called convective range of isotropic turbulence, which is analogous to the inertial range for hydrodynamic turbulence. The experimental situation of this fundamental law is similar to that of the 4/5ths law. On the one hand, indications of this law appear for rather small values of Péclet number. On the other hand, formation of the convective (inertial) range itself is quite slow with increasing Péclet number. Since the qualitative characteristics of the Yaglom law are similar to those of Kolmogorov's, we will be brief in describing overlapping aspects.

The diffusion-convection equation for a passive scalar with random 'force' (source) $f(\mathbf{x}, t)$ is

$$\frac{\partial \theta}{\partial t} + u_j \frac{\partial \theta}{\partial x_j} = \kappa \frac{\partial^2 \theta}{\partial x_j^2} + f(\mathbf{x}, t), \quad (2.15)$$

where κ is the molecular diffusivity. As before, we assume Gaussianity and δ -correlation in time for the forcing. The Gaussian forces with zero mean are defined by their second-rank correlation

$$\langle f(\mathbf{x} + \mathbf{r}, t + \tau) f(\mathbf{x}, t) \rangle = F(\mathbf{r}) \delta(\tau). \quad (2.16)$$

It is known that the mixed (longitudinal) structure function of third order

$$S_3^{u\theta}(r) = \langle \Delta u_r (\Delta \theta_r)^2 \rangle \quad (2.17)$$

is related to the second-order structure function $S_2^\theta(r) = \langle (\Delta \theta_r)^2 \rangle$ by the equation

$$S_3^{u\theta} = 2\kappa \frac{dS_2^\theta}{dr} - \frac{2}{r^2} \int_0^r x^2 F(x) dx. \quad (2.18)$$

Let us rewrite (2.18) formally as

$$S_3^{u\theta} = -\frac{2}{r^2} \int_0^r x^2 \tilde{F}(x) dx, \quad (2.19)$$

where we define generalized input rate for the variance of the passive scalar as

$$\tilde{F}(x) \equiv \left(F(x) - \frac{\kappa}{x^2} \frac{d(x^2 dS_2^\theta/dx)}{dx} \right). \quad (2.20)$$

Let us now assume the existence of a local maximum of the generalized input rate, i.e. a local maximum of $\tilde{F}(x)$ at $x = x_m$ (where $\eta < x_m < L_\theta$, η being the molecular diffusion scale and L_θ the integral scale). From dimensional considerations

$$\tilde{F}(x) = \chi \psi(x/x_m) \quad (2.21)$$

where $\psi(x/x_m)$ is a dimensionless function. The inertial (convective) range is expected to appear in the flow for sufficiently large Péclet numbers (Monin & Yaglom 1975). We assume that $\psi(x/x_m) = \psi(1) = \text{const}$ in this range and that, for r within that range, this particular value of ψ gives the main contribution to the integral (2.19). From (2.19) follows the result that

$$S_3^{u\theta}(r) = -\frac{2}{3} \chi \psi(1) r. \quad (2.22)$$

Taking into account the Yaglom law (2.14) for the convective range, we obtain

$$\psi(1) = 2. \quad (2.23)$$

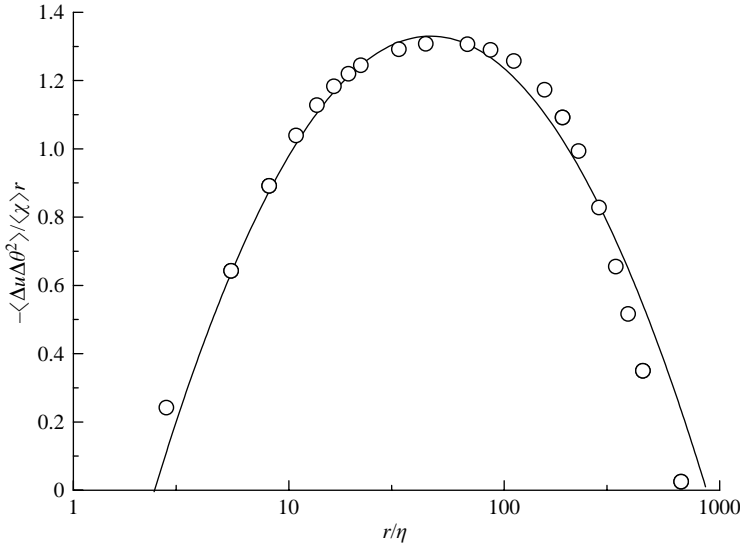


FIGURE 8. Mixed third-order structure function $S_3^{u\theta}/\chi r$ against $\log r$. The DNS data of Watanabe & Gotoh (2004) ($P_\lambda = 258$) are shown as circles (η is the Kolmogorov scale). The solid parabola corresponds to (2.26) with the first two terms.

If the ideal convective range has not yet appeared, we may use a logarithmic expansion of the generalized input rate in a vicinity of its maximum:

$$\tilde{F}(x) = \tilde{F}(x_m) - \beta_1(\ln(x/x_m))^2 + \dots + \beta_{n-1}(\ln(x/x_m))^n + \dots \tag{2.24}$$

(with $\beta_1 > 0$). Again, this logarithmic expansion is the key ingredient of our analysis. It would be highly instructive if the logarithmic expansion could be derived at least for a model of the passive scalar such as the Kraichnan model (see e.g. Falkovich, Gawedzki & Vergassola 2001), but this is an unfinished task for now.

Taking into account (2.14) and (2.23), it is useful to rewrite (2.24) in the form

$$\tilde{F}(x) \simeq 2\langle\chi\rangle E[1 - F((\ln(x/x_m))^2 + \dots)], \tag{2.25}$$

where E and F are dimensionless constants. Then substituting (2.25) into (2.19) and assuming the symmetry of the $S_3^{u\theta}(r/r_m)$ in a vicinity of its maximum position $r = r_m$ we obtain

$$S_3^{u\theta}(r) = -\frac{4}{3}\langle\chi\rangle r G[1 - H_2(\ln r/r_m)^2 + H_4(\ln r/r_m)^4 + \dots], \tag{2.26}$$

where $r_m \propto x_m$, $G(\approx 1)$, H_2 and H_4 are constants.

Figure 8 shows $-S_3^{u\theta}/\chi r$ against $\log r$ for the DNS data of homogeneous isotropic turbulence described in Watanabe & Gotoh (2004), Péclet number $P_\lambda = 258$. The solid parabola follows (2.26) with the first two terms ($G \simeq 1$). Figure 9 shows analogous data obtained for $P_\lambda = 427$, also from Watanabe & Gotoh (2004). The solid curve is the best fit to (2.26) with the next term included ($G \simeq 0.96$).

The discussion concerning the Kolmogorov law is relevant here as well. It is, however, clear that one could approximate the measured $S_3^{u\theta}(r)$ in the ‘convective range’ for any finite Péclet numbers by taking an increased number of terms in (2.25) (and, consequently, in (2.26)). This approach could complement the idea of the ideal convective range valid for $P_\lambda = \infty$.

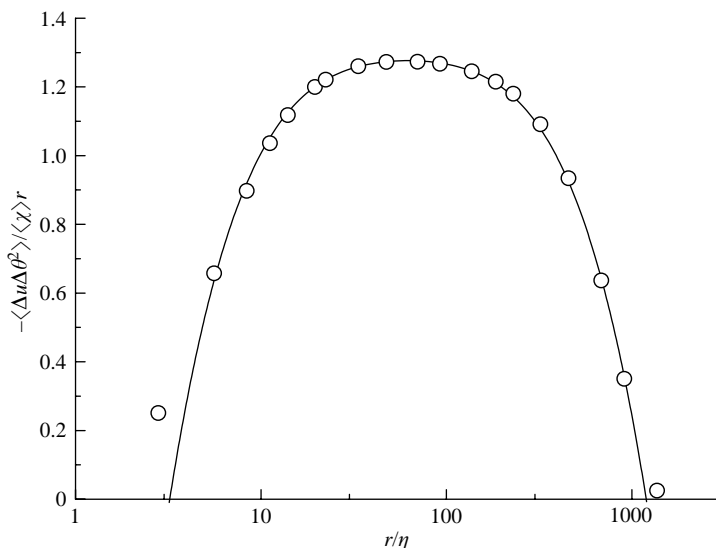


FIGURE 9. As in figure 8 but for $P_\lambda = 427$. The solid curve corresponds to the approximation (2.26) with the first three terms.

3. Wall-bounded turbulence

Very close to the surface in wall-bounded flows such as pipes, channels and boundary layers, the mean velocity varies linearly with the wall-normal distance (e.g. Laufer 1954). Further away from the surface, the traditional understanding has been that the variation is logarithmic (Prandtl 1952). In a series of publications (e.g. Barenblatt 1993; Barenblatt *et al.* 1997), it has been proposed that power-law variation is more appropriate.† Even further out in the flow, the so-called wake function (Coles & Hirst 1968) is thought to codify experimental data. This section does not elucidate any of this work directly, but we merely use logarithmic expansions to construct an explicit expression for the mean velocity distribution near the position of maximum Reynolds shear stress, y_m .

Let us start with the exact equation

$$-\langle uv \rangle^+ = dU^+/dy^+ + (1 - y^+/R^+), \quad (3.1)$$

valid for pipes and channel flows, in which we have used the standard notation: u and v are velocity fluctuations in the streamwise and wall-normal directions x and y , respectively, $U(y)$ is the mean velocity in the direction x , R is the pipe radius or the channel half-height, and the suffix $+$ indicates normalization by wall variables u_τ and ν , which represent, respectively, the friction velocity and the (kinematic) fluid viscosity. Elementary considerations show that the turbulent stress term $-\langle uv \rangle^+$ increases cubically with y^+ very close to the wall; it changes rapidly into a form that has not been studied carefully so far, before attaining its maximum value; it subsequently drops off to zero as the flow centreline is approached further outwards. The position of the maximum in the Reynolds shear stress, y_m , is empirically known

† Power laws themselves have been around for much longer, but the framework of intermediate asymptotics emphasized by this modern work is new.

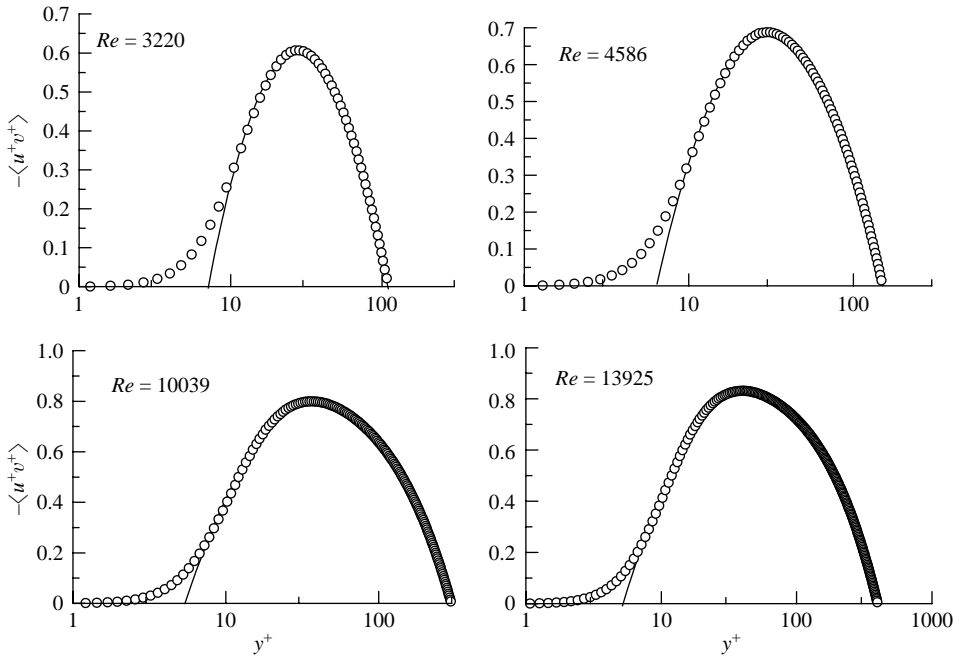


FIGURE 10. Plots of the Reynolds shear stress from the direct numerical simulations of a channel flow (Iwamoto, Suzuki & Kasagi 2002), for four different Reynolds numbers, Re , based on the bulk mean velocity and the width of the channel. The data have been fitted by the two-term expansion (3.3). The fit is very good for $y^+ > 10$.

(Sreenivasan & Sahay 1997) to obey

$$y_m^+ \approx 1.87(R^+)^{1/2}. \tag{3.2}$$

Such a fit has been proposed for some time (Long & Chen 1981; Sreenivasan 1987), but the multiplicative constant has been slightly different in each work because of the uncertainty associated with identifying y_m from the measured data. The distribution of $-\langle uv \rangle^+$ in pipe and channel flows has been obtained by numerically differentiating the measured mean velocity distribution and using (3.1), and so (3.2) is not affected by the inaccuracies of measuring the Reynolds shear stress.

Let us expand $-\langle uv \rangle^+$ around y_m^+ . Sreenivasan & Sahay (1997) have undertaken this exercise already but had not appreciated the importance of expanding $-\langle uv \rangle^+$ in terms of the logarithm of the distance from y_m^+ . This appears to be the appropriate expansion because the number of hierarchical scales up to the height y^+ in the wall layer is of the order $\ln y^+$. We may then write

$$-\langle uv \rangle^+ = k[1 - \gamma_1(\ln(y^+/y_m^+))^2 + \dots + \gamma_n(\ln(y^+/y_m^+))^n + \dots]. \tag{3.3}$$

Here, the unknown constants $\gamma_1 \dots \gamma_n$ are thought to be independent of the Reynolds number, at least when it is high enough, and $k \rightarrow 1$ as $Re \rightarrow \infty$.

The two-term (parabolic) fit works well for all Reynolds numbers shown in figure 10, roughly for $y^+ \geq 10$. The low end of the fitted region more or less borders the buffer region. Substituting (3.3) in (3.1), and retaining only the first two terms in the expansion (3.3), we obtain

$$U^+ = \text{const} + y^+[g(y^+) - (y^+/2R^+)], \tag{3.4}$$

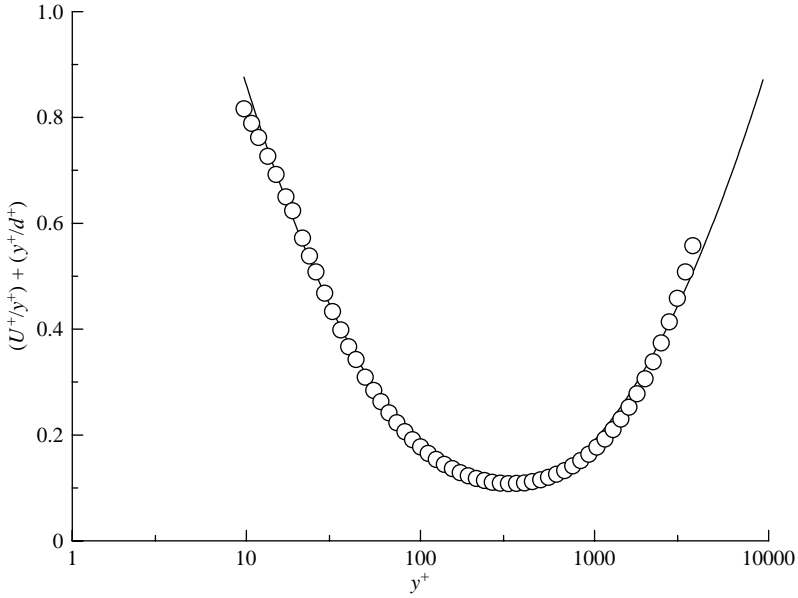


FIGURE 11. A plot of $U^+/y^+ + y^+/d^+$ against y^+ in semi-log scales (circles), for $Re = 144\,580$, where Re is based on the mean velocity and the pipe diameter. The data are from McKeon *et al.* (2004). The solid parabola corresponds to equation (3.8).

where

$$g(y^+) = p_0 + p_1[\ln(y^+/y_1)]^2, \tag{3.5}$$

with

$$p_0 = 1 - k + k\gamma_1, \quad p_1 = k\gamma_1, \quad y_1 = ey_m^+. \tag{3.6}$$

The expression (3.4) is technically not expected to be valid all the way to the wall (see figure 10), but we can be somewhat rough and impose the no-slip condition $U^+ = 0$ at $y^+ = 0$ to obtain

$$U^+ = y^+[g(y^+) - y^+/d^+], \tag{3.7}$$

where $d^+ = 2R^+$. In order to compare the last equation directly with experimental data, it is useful to rewrite it in the form

$$U^+/y^+ + y^+/d^+ = g(y^+) = p_0 + p_1[\ln(y^+/y_1)]^2. \tag{3.8}$$

If the present considerations are valid, the left-hand side of (3.8) must show a parabolic variation with respect to y^+ in logarithmic coordinates.

We show in figure 11 the recent data of McKeon *et al.* (2004) for one Reynolds number. The solid parabola corresponds to (3.8). The agreement with the data is excellent almost all the way to y^+ of the order 10 towards the wall, and to y^+ of the order 1000 or more outwards – in fact, almost all the way to the centreline.

The following remarks seem useful. In the traditional picture, the Reynolds shear stress attains a constant value of unity in an intermediate region, this being the fundamental factor leading to the logarithmic law (in analogy with the Kolmogorov ‘inertial range’ picture considered in §2; see e.g. Tennekes & Lumley 1972). If, on the other hand, the maximum in $-\langle uv \rangle^+$ can indeed be identified at all Reynolds numbers, this feature would suggest a second viscous-dominated region around y_m^+ , and has to be taken into account in some way. Such considerations introduce new

elements in the asymptotic analysis of the wall-bounded flows, and were the subject of Sreenivasan & Sahay (1997). Alternatively, it is possible that the relation (3.2) holds only for ‘low’ Reynolds numbers in which case the present considerations hold only that range of Reynolds numbers. It is possible that y_m^+ remains fixed beyond a certain Reynolds number so the major influence of increasing the Reynolds number further is simply to fill up more and more of the flat part of the Reynolds stress to the right of y_m^+ . At present, we do not have sufficiently good data to choose one scenario over the other.

4. The clustering phenomenon

4.1. The telegraph approximation and the cluster exponents

The nature of scaling laws in turbulence is still a challenging problem. Even the basic cornerstone of the phenomenology of turbulence, namely Kolmogorov’s $-5/3$ spectral form for locally isotropic and incompressible turbulence, has not been obtained from the Navier–Stokes equations. Properties of intermittency are similarly beyond the reach of theory at present (although considerable progress has been made for passive scalars, see e.g. Falkovich *et al.* 2001). Intermittency consists of two aspects: different events cluster together so their density in space is uneven, and events of highly variable amplitudes are dispersed sporadically in space. In general, it has not been possible to separate the clustering effect from the amplitude effect. Here, we suggest a simplification using the so-called telegraph approximation for the velocity to separate the two effects, and discuss how the inverse logarithmic expansion appears naturally for dissipation intermittency.

The telegraph approximation is generated from the measured signal by setting the fluctuation magnitudes to 1 or 0 depending on whether the magnitude exceeds the mean value. Formally, for the fluctuation of measured quantity $u(t)$ (with zero mean), the telegraph approximation $u^*(t)$ is constructed as

$$u^*(t) = \frac{1}{2} \left(\frac{u(t)}{|u(t)|} + 1 \right). \quad (4.1)$$

By definition, u^* can equal either 1 and 0. Figure 12 illustrates the basic idea schematically.

In turbulence, the energy dissipation (or, more precisely, a component of it) is obtained by squaring the derivative of the velocity signal. As is well known (e.g. Grant, Stewart & Moilliet 1962; Meneveau & Sreenivasan 1991), the result at high Reynolds number is a highly intermittent quantity. For the telegraph approximation of the velocity, however, the ‘derivative’ (interpreted as the limit of differences) has a magnitude of ± 1 , situated at the shoulders of the pulses, and the equivalent of the dissipation is then a train of spikes of unity magnitude. Since there is no change in magnitude from one spike to another, the entire manifestation of intermittency is due to the tendency of the spikes to cluster together. This addresses one part of intermittency without involving the amplitude variability.†

† Another reason for the interest in the telegraph approximation is that it could provide a motivation for using symbolic dynamics to study Navier–Stokes equations. If some rigorous results could be derived by this means, one would then be able to make a more direct connection between the equations and the scaling properties to be discussed in this section. A more detailed discussion of these issues will be published separately.

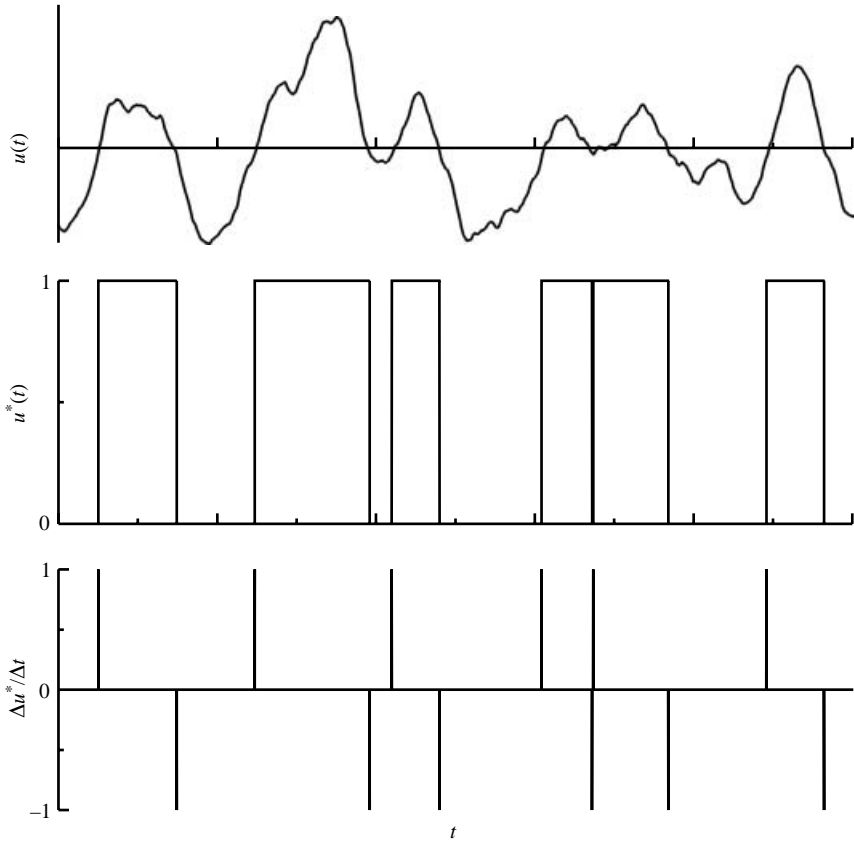


FIGURE 12. Schematic of the velocity fluctuations signal and its telegraph approximation. The bottom figure shows the ‘derivative’ of the telegraph approximation.

In particular, let us construct, as is common for the energy dissipation, a running average within a time interval τ of the number of spikes generated from the telegraph signal; this quantity is simply equal to N_τ , which is the average number of zero-crossing points in the interval τ . Let us denote fluctuations of the running average by $N'_\tau = N_\tau - \langle N_\tau \rangle$, where the brackets mean long-time average. We now inquire about the scaling of the variance – that is, the Reynolds-number variation of the cluster exponent μ^* in the power-law relation

$$\langle N'^2_\tau \rangle^{1/2} \sim \tau^{\mu^*}. \tag{4.2}$$

The exponents for $\langle N'^q_\tau \rangle^{1/q}$ will also be μ^* for all q because there is no amplitude variability in the telegraph approximation. (This has been checked empirically as well.)

4.2. Inverse logarithmic expansion

Data analysis has been performed using velocity signals measured at several Reynolds numbers and the cluster exponents have been obtained. After having experimented with different forms of variations with the microscale Reynolds number R_λ , we found that the best fit was obtained when the data were correlated with $\ln R_\lambda$. The first two terms in the expansion

$$\mu^*(\ln R_\lambda) = q_0 + \frac{q_1}{\ln R_\lambda} + \frac{q_2}{(\ln R_\lambda)^2} + \dots \tag{4.3}$$

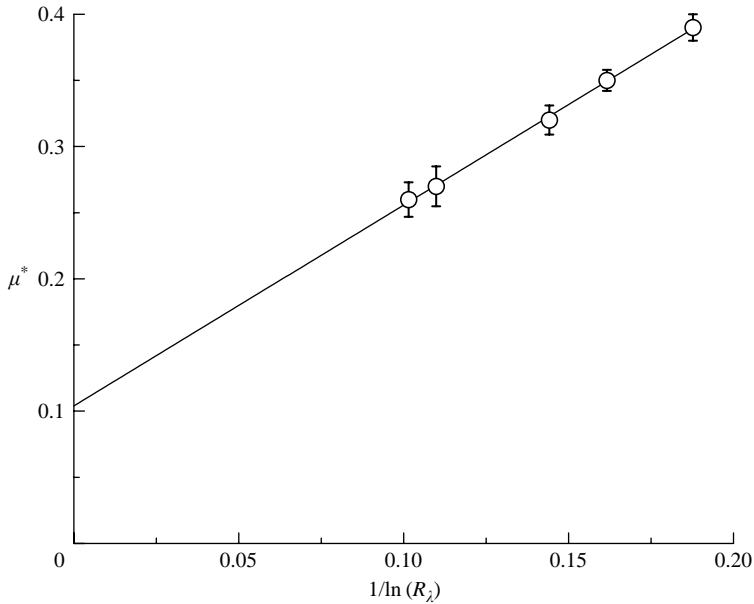


FIGURE 13. Cluster exponent μ^* (circles) for the velocity signal at different values of Reynolds number ($200 < R_\lambda < 20\,000$) against $1/\ln R_\lambda$.

agree very well with the calculated values of μ^* for $200 < R_\lambda < 20\,000$. Figure 13 shows that the best linear fit is

$$\mu^*(\ln R_\lambda) \simeq 0.1 + \frac{3/2}{\ln R_\lambda}, \tag{4.4}$$

which means that

$$\lim_{R_\lambda \rightarrow \infty} \mu^* \simeq 0.1. \tag{4.5}$$

There is finite clustering effect even in the limit of infinite Reynolds number. Again, $\ln R_\lambda$ seems to be the appropriate expansion parameter because the number of steps in the energy cascade is proportional to $\ln R_\lambda$. (In one interpretation (Sreenivasan & Stolovitzky 1995), the number of ‘particles’ on which one can do statistical mechanics is equal to $\log_2 R_\lambda$.)

4.3. Clustering of passive scalar fluctuations

Clustering of small scales of passive scalar in turbulent flows can also be characterized by a corresponding cluster exponent. The principal result, which will be stated without evidence for the sake of brevity, is that the coefficients q_0 and q_1 in the corresponding expansion for the cluster exponent are approximately 0.07 and 3/2, respectively. The smaller value of q_0 , in comparison with that for velocity, suggests that there is a greater tendency for scalar fluctuations to cluster together.

5. Flatness of the velocity derivative

Observations show that the turbulent velocity becomes ‘rougher’ with increasing Reynolds number, but it is generally thought that the tendency to form singularities is

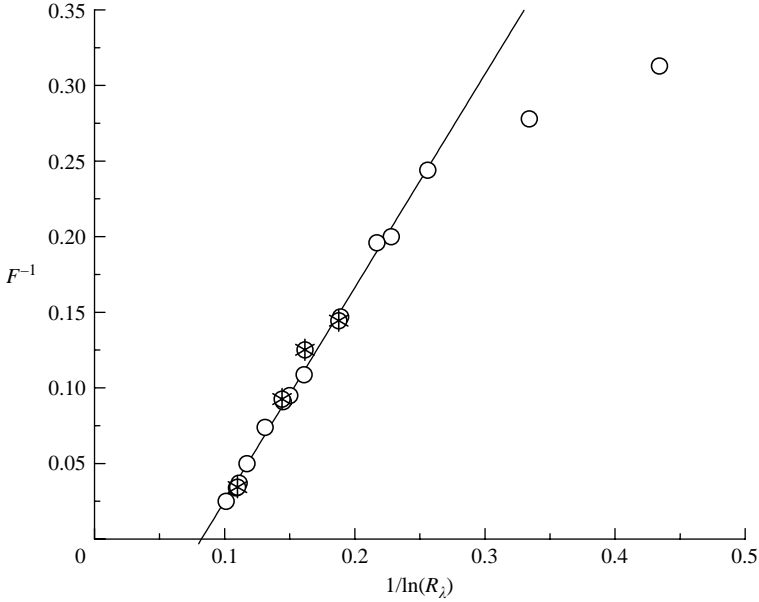


FIGURE 14. Inverse flatness data (circles and crosses) against inverse $\ln R_\lambda$. The solid straight line (the best fit) indicates the two-term expansion (5.1).

mitigated by the smoothing effects of viscosity. From an experimentalist’s perspective, if the singularities occur at all, they should be observed in velocity gradients (or combinations thereof), and statistical quantities such as the flatness (i.e. the normalized fourth-order moment) of the so-called longitudinal velocity derivative must detect them. We make a few remarks on this subject in the context of inverse logarithmic expansions. The experimental data available a few years ago were collected by Sreenivasan & Antonia (1997).

It is usually thought that the flatness increases as a power-law in R_λ , for $R_\lambda > 100$ or so. This range of R_λ is thus thought to be fully developed. In reality, however, the data do not confirm a flawless power law in any Reynolds-number range and are open to different interpretations (e.g. Tabeling & Willaime 2002; Gylfason, Ayyalasomayajulu & Warhaft 2004). A new interpretation is attempted below using an inverse log expansion (for a few more details, see Sreenivasan & Bershadskii 2005).

5.1. Interpretation using logarithmic expansions

Figure 14 shows inverse flatness F^{-1} (from the local average fit of the data from Sreenivasan & Antonia 1997) against $1/\ln(R_\lambda)$ (circles). New data from wind tunnel (Pearson *et al.* 2002) and atmospheric surface layer measurements (Sreenivasan & Dhruva 1998) are added (crosses). The straight line shows the two-term approximation of the inverse logarithmic expansion

$$F(x)^{-1} = q_0 + q_1x + \dots + q_nx^n + \dots \tag{5.1}$$

with

$$x = 1/\ln(R_\lambda). \tag{5.2}$$

This fit is good from $R_\lambda \approx 50$ (which is on the order of the minimum Reynolds number at which turbulence-like behaviour sets in (Sreenivasan 1984)) and describes

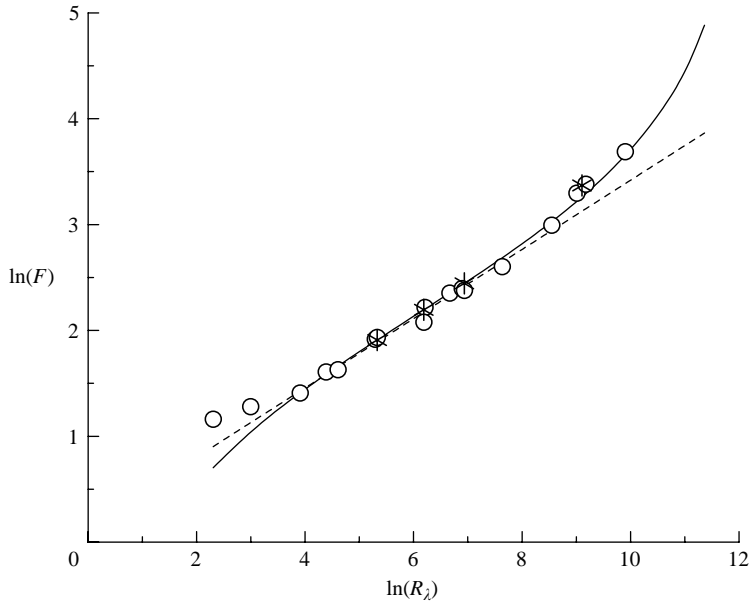


FIGURE 15. The same as in figure 14 but in the usually used log-log scales. The solid curve is ‘critical’ approximation (5.3) and the dashed line the conventional power law.

all the measured data up to $R_\lambda \approx 20\,000$. The figure shows that $q_0 < 0$, indicating the possibility of a finite-Reynolds-number singularity of the flatness. In this situation, to apply the expansion (5.1) as a Maclaurin series, one can do an analytic continuation of the variable F^{-1} in the negative area defining $F(0)^{-1} \equiv q_0$, $dF^{-1}/dx|_{x=0} \equiv q_1$, etc. (In the theory of critical phenomena, analytic continuations are produced even in the complex plane.) The linear approximation of the $F(x)^{-1}$ results in critical-like expression for

$$F(x) \sim (x - x_c)^{-1} \tag{5.3}$$

in a certain vicinity of the ‘critical’ point $x_c = -q_0/q_1$.

Extrapolating this fit one can find the ‘critical’ value $x_c = \ln R_\lambda^{(c)} \simeq 12.6 \pm 1.5$, as the intersection point of the fitting straight line with the horizontal axis. This gives a ‘critical’ Reynolds number $R_\lambda^{(c)}$ of about 300 000. While the error bar in $1/\ln R_\lambda^{(c)}$ seems reasonable, it translates to huge error bars of between 66 000 and 1 300 000 in the value of $R_\lambda^{(c)}$ itself.

A slightly different perspective on the topic is provided in figure 15, which compares the smoothed data (circles) with the ‘critical’ approximation (5.3) (solid curve) as well as the conventional power law used in log-log coordinates (dashed straight line). Even though there is a slight suggestion that the data prefer the ‘critical’ line to the pure power-law (towards the upper end of R_λ), one needs an order of magnitude higher R_λ in order to determine unambiguously whether the data will follow the traditionally expected power law or the critical behaviour. While such Reynolds numbers are outside the present experimental capability – and also outside terrestrial experience – the issue is of fundamental theoretical interest.

There is one possibility of testing this notion within our present capabilities. The velocity measurements, from which the derivative flatness is computed, have been made typically with a resolution on the order of the Kolmogorov scale. It is now known (Sreenivasan 2004; Yakhot & Sreenivasan 2005) that the required resolution

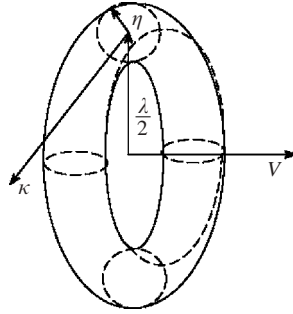


FIGURE 16. The vortex ring and its velocity.

becomes more stringent as the Reynolds number increases. There is some evidence to suggest that the flatness measured with adequate resolution reveals a tendency to curve upwards. If this tendency is shared by the higher- R_λ data, the evidence for the critical scenario will be stronger. Adequately resolved flatness measurements at high R_λ are therefore an urgent necessity.

6. Discussion

In this paper, we have discussed a few examples to illustrate the range of problems for which logarithmic expansions are useful. To the evidence presented, one can add other instances, e.g. those involving thermal convection. Considering the present examples in conjunction with others in which log-expansions have already been carried out (e.g. Castaing *et al.* 1990; Barenblatt & Goldenfeld 1995; Dubrulle 1996), the totality of evidence appears strong. Yet all the evidence is empirical. It is therefore useful to seek a logical explanation for the appearance of logarithmic expansions applicable in diverse turbulence problems.

Thin vortex tubes (or filaments) are the ubiquitous hydrodynamical elements of turbulent flows at high Reynolds numbers (Küchemann 1965; Saffman 1968; Chorin 1994). Therefore, it is natural to seek a generic property of vortex filaments to provide the required physical mechanism. We examine their stability in three-dimensional space, in particular the propensity of a linear vortex to develop ‘kinks’. To estimate the velocity of such a kink, let us first recall (Batchelor 1967) that a ring vortex propagates with a speed v that is related to its diameter λ and strength Γ through

$$v = \frac{\Gamma}{2\pi\lambda} \ln \left(\frac{\lambda}{2\eta} \right), \quad (6.1)$$

where η is the radius of the core of the ring and $\lambda/2\eta \gg 1$ (see figure 16). If, for instance, a linear vortex develops a kink with a radius of curvature $\lambda/2$, the velocity perpendicular to the plane of the kink, generated by self-induction, can be calculated using (6.1).

One can guess (see Saffman 1968) that in a turbulent environment, the most unstable mode of a thin vortex tube of length L (integral scale) and radius η (Kolmogorov scale), will be of the order of the Taylor microscale, λ . Then, the characteristic velocity of the spatial scale λ can be estimated from (6.1). Noting that the Taylor-microscale Reynolds number is defined as

$$R_\lambda = \frac{v_0\lambda}{\nu}, \quad (6.2)$$

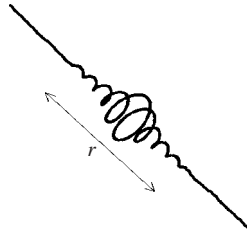


FIGURE 17. Vortex filament instability and the wave packet of scale r .

where v_0 is the root-mean-square value of a component of velocity, it appears that the velocity that is more relevant (at least from the point of view of vortex instabilities) for the spatial scale λ is not v_0 but v given by (6.1). The corresponding effective Reynolds number should be obtained by the renormalization of the characteristic velocity in (6.2), as

$$R_\lambda^{eff} = \frac{v\lambda}{\nu} \sim \frac{\Gamma}{2\pi\nu} \ln\left(\frac{\lambda}{2\eta}\right). \tag{6.3}$$

It can be readily shown from definitions that

$$\frac{\lambda}{\eta} = G R_\lambda^{1/2}, \tag{6.4}$$

where $G = 15^{1/4} \simeq 2$. Hence

$$R_\lambda^{eff} \sim \frac{\Gamma}{4\pi\nu} \ln(R_\lambda). \tag{6.5}$$

The strength Γ can be estimated as

$$\Gamma \sim 2\pi v_\eta \eta, \tag{6.6}$$

where $v_\eta = v/\eta$ is the velocity scale for the Kolmogorov scale η . Substituting (6.6) into (6.5) we obtain

$$R_\lambda^{eff} \sim \ln R_\lambda. \tag{6.7}$$

Thus, for turbulence processes determined by vortex instabilities, the relevant dimensionless characteristic is $\ln R_\lambda$ rather than R_λ . This is a plausible justification for the relevance of expansions in terms of the inverse logarithm of the microscale Reynolds number.

We now turn to the logarithmic expansions used in the first part of the paper, where the finite-size corrections to the ideal scaling laws were considered as functions of $\ln(r/r_m)$. A plausible explanation for this procedure is as follows. In the finite-size computations, the cut-off corrections from above to Δu_r arising from vortex instabilities (see figure 17) can be calculated by the ‘local induction’ approximation to the Biot-Savart formula (Batchelor 1967). This suggests that, at the level of the present approximation, contributions to the velocity fluctuation in the immediate vicinity of a given point on the filament, arising from distances $r \gg \eta$, can be neglected. The cut-off from below is provided by the core radius η of the vortex. Then the dynamics of the vortex filament obey the equation

$$\frac{d\mathbf{X}}{dt} = \frac{\Gamma}{4\pi} \left\{ \ln\left(\frac{r}{\eta}\right) \right\} \gamma \mathbf{b}, \tag{6.8}$$

where \mathbf{X} is the position vector of a point on the filament, γ is the local curvature, and \mathbf{b} is the unit binormal vector of the filament. In this approximation, since the

dependence on r is exclusively determined by the logarithmic term in the right-hand side of (6.8), a correction function to the turbulent velocity fluctuations, related to the finite-size effects, is also a function of $\ln(r/\eta)$.

Let us now consider a finite-size correction function $f(\ln(r/\eta))$ with its maximum at $r = r_m$ (see §2). This function can be rewritten as $f(\ln(r/\eta)) \equiv f(\ln(r/r_m) + \ln(r_m/\eta))$. In the vicinity of the maximum, we have

$$\ln \frac{r_m}{\eta} \gg \ln \frac{r}{r_m}. \quad (6.9)$$

Therefore we can effectively use a power series expansion in this vicinity:

$$f\left(\ln \frac{r}{\eta}\right) \equiv f\left(\ln \frac{r}{r_m} + \ln \frac{r_m}{\eta}\right) = a_0 + a_2 \left(\ln \frac{r}{r_m}\right)^2 + \cdots + a_n \left(\ln \frac{r}{r_m}\right)^n + \cdots, \quad (6.10)$$

where

$$a_0 = f\left(\ln \frac{r_m}{\eta}\right), \quad a_n = \frac{1}{n!} \left. \frac{d^n f(x)}{dx^n} \right|_{x=\ln(r_m/\eta)}.$$

That is, all turbulent processes – for which the instability of the vortex filaments determines finite-size effects – can be expanded in terms of logarithmic power expansions. Equation (6.9) provides a condition of effective applicability of such expansions. Taking into account that the effective length of the vortex filament is $\sim L$, one can roughly estimate $r_m \sim (L\eta)^{1/2} \sim R_\lambda^{3/4}\eta$. This result is in agreement with the scaling shown in figure 5.

In summary, we have argued here that, instead of expansions in terms of powers of the Reynolds number or its inverse, those in terms of powers of the logarithm of the Reynolds number or its inverse are more generic, at least in those instances where vortex instabilities are involved. Since most turbulent processes are likely to be related to such instabilities, it is reasonable to speculate that such expansions are natural for turbulence theories. We have discussed a few instances where they have proved to be useful, and there is little doubt that more are likely to be identified.

We thank T. Gotoh, K. Iwamoto, B. McKeon, C. Meneveau, B.R. Pearson and P.K. Yeung for providing the data of their numerical simulations and experiments.

REFERENCES

- BARENBLATT, G. I. 1993 Scaling laws for fully developed turbulent shear flows. *J. Fluid Mech.* **248**, 513–520.
- BARENBLATT, G. I., CHORIN, A. J. & PROSTOKISHIN, V. M. 1997 Scaling laws for fully developed turbulent flows in pipes. *Appl. Mech. Rev.* **50**, 413–429.
- BARENBLATT, G. I. & GOLDENFELD, N. 1995 Does fully developed turbulence exist? Reynolds number independence versus asymptotic covariance. *Phys. Fluids* **7**, 3078–3082.
- BATCHELOR, G. K. 1951 Pressure fluctuations in isotropic turbulence. *Proc. Camb. Phil. Soc.* **47**, 359–374.
- BATCHELOR, G. K. 1967 *An Introduction to Fluid Dynamics*. Cambridge University Press.
- CASTAING, B., GAGNE, Y. & HOPFINGER, E. J. 1990 Velocity probability density-functions of high Reynolds-number turbulence. *Physica D* **46**, 177–200.
- CHORIN, A. J. 1994 *Vorticity and Turbulence*. Springer.
- COLES, D. E. & HIRST, E. A. 1969 Computation of turbulent boundary layers. *Proc. 1968 AFOSR-IFP-Stanford Conference*. Thermosciences Division, Stanford University.
- DONZIS, D. A., SREENIVASAN, K. R. & YEUNG, P. K. 2005 Scalar dissipation rate and dissipative anomaly in isotropic turbulence. *J. Fluid Mech.* **532**, 199–216.

- DUBRULLE, B. 1996 Anomalous scaling and generic structure function in turbulence. *J. de Phys. II*, **6**, 1825–1840.
- FALKOVICH, G., GAWEDZKI, K. & VERGASSOLA, M. 2001 Particles and fields in fluid turbulence. *Rev. Mod. Phys.* **73**, 913–975.
- GAGNE, Y., CASTAING, B., BAUDET, CH. & MALECOT, Y. 2004 Reynolds dependence of third-order velocity structure functions. *Phys. Fluids* **16**, 482–485.
- GOTOH, T., FUKAYAMA, D. & NAKANO, T. 2002 Velocity field statistics in homogeneous steady turbulence obtained using a high-resolution direct numerical simulation. *Phys. Fluids* **14**, 1065–1081.
- GRANT, H. L., STEWART, R. W. & MOILLIET, A. 1962 Turbulence spectra from a tidal channel. *J. Fluid Mech.* **12**, 211–268.
- GYLFASON, A., AYYALASOMAYAJULA, S. & WARHAFT, Z. 2004 Intermittency, pressure and acceleration statistics from hot-wire measurements in wind-tunnel turbulence. *J. Fluid Mech.* **501**, 213–229.
- IWAMOTO, K., SUZUKI, Y. & KASAGI, N. 2002 Reynolds number effect on wall turbulence: toward effective feedback control *Intl J. Heat Fluid Flow* **23**, 678–689.
- KANG, H. S., CHESTER, S. & MENEVEAU, C. 2003 Decaying turbulence in an active-grid-generated flow and comparisons with large-eddy simulation. *J. Fluid Mech.* **480**, 129–160.
- KANEDA, Y., ISHIHARA, T., YOKOKAWA, M., ITAKURA, K. & UNO, A. 2003 Energy dissipation rate and the energy spectrum in high resolution direct numerical simulations of turbulence in a periodic box. *Phys. Fluids* **15**, L21–L24.
- KOLMOGOROV, A. N. 1941 Dissipation of energy in locally isotropic turbulence. *Dokl. Akad. Nauk. SSSR* **32**, 16–18.
- KRAICHNAN, R. H. 1968 Small-scale structure of a scalar field convected by turbulence. *Phys. Fluids* **11**, 945–953.
- KÜCHEMANN, D. 1965 Report on the IUTAM symposium on concentrated vortex motion in fluids. *J. Fluid Mech.* **21**, 1–20.
- LAUFER, J. 1954 The structure of turbulence in fully developed pipe flow. *NACA Rep.* 1174.
- LONG, R. R. & CHEN, T. C. 1981 Experimental evidence for the existence of mesolayer in turbulent systems. *J. Fluid Mech.* **105**, 19–59.
- MCKEON, B. J., LI, J., JIANG, W., MORRISON, J. F. & SMITS, A. J. 2004 Further observations on the mean velocity distribution in fully developed pipe flow. *J. Fluid Mech.* **501**, 135–147.
- MENEVEAU, C. & SREENIVASAN, K. R. 1991 The multifractal nature of the turbulent energy dissipation. *J. Fluid Mech.* **224**, 429–484.
- MONIN, A. S. & YAGLOM, A. M. 1975 *Statistical Fluid Mechanics*, Vol. 2. MIT Press.
- MOISY, F., TABELING, P. & WILLAIME, H. 1999 Kolmogorov equation in a fully developed turbulence experiment. *Phys. Rev. Lett.* **82**, 3994–3997.
- NOVIKOV, E. A. 1965 Functionals and random-force method in turbulence theory. *Sov. Phys. JETP* **20**, 1290–1294.
- PEARSON, B. R., KROGSTAD, P.-A. & VAN DE WATER, W. 2002 Measurements of the turbulent energy dissipation rate. *Phys. Fluids* **14**, 1288–1290.
- PRANDTL, L. 1952 *Essentials of Fluid Mechanics*. Hafner Publishing, New York.
- SAFFMAN, P. G. 1968 Lectures on homogeneous turbulence. In *Topics in Nonlinear Physics* (ed. N. J. Zabusky), pp. 485–614. Springer.
- SREENIVASAN, K. R. 1984 On the scaling of the turbulence energy dissipation rate. *Phys. Fluids* **27**, 1048–1051.
- SREENIVASAN, K. R. 1987 A unified view of the origin and morphology of the turbulent boundary layer structure. In *Turbulence Management and Relaminarisation* (ed. H. W. Liepmann & R. Narasimha), pp. 37–61. Springer.
- SREENIVASAN, K. R. 2004 Possible effects of small-scale intermittency in turbulent reacting flows. *Flow, Turbulence & Combust.* **72**, 115–131.
- SREENIVASAN, K. R. & ANTONIA, R. A. 1997 The phenomenology of small-scale turbulence. *Annu. Rev. Fluid Mech.* **29**, 435–475.
- SREENIVASAN, K. R. & BERSHADSKII, A. 2005 Does the flatness of the velocity derivative blow up at a finite Reynolds number? *Pramana* **64**, 939–945.
- SREENIVASAN, K. R. & DHRUVA, B. 1998 Is there scaling in high-Reynolds-number turbulence? *Prog. Theor. Phys. Supp.* **130**, 103–120.

- SREENIVASAN, K. R. & SAHAY, A. 1997 The persistence of viscous effects in the overlap region, and the mean velocity in turbulent pipe and channel flows. In *Self-Sustaining Mechanism of Wall Turbulence* (ed. R. L. Panton), pp. 253–271 Computational Mechanics Publications, Southampton and Boston.
- SREENIVASAN, K. R. & STOLOVITZKY, G. 1995 Turbulent cascades. *J. Statist. Phys.* **78**, 311–331.
- STOLOVITZKY, G., SREENIVASAN, K. R. & JUNEJA, A. 1993 Scaling functions and scaling exponents in turbulence. *Phys. Rev. E* **48**, R3217–R3220.
- TABELING, P. & WILLAIME, P. H. 2002 Transition at dissipative scales in large-Reynolds-number turbulence *Phys. Rev. E* **65**, 066301.
- TENNEKES, H. & LUMLEY, J. L. 1972 *A First Course in Turbulence*. MIT Press.
- WATANABE, T. & GOTOH, T. 2004 Statistics of a passive scalar in homogeneous turbulence. *New J. Phys.* **6**, Art. 40.
- YAKHOT, V. & SREENIVASAN, K. R. 2005 Anomalous scaling of structure functions and dynamic constraints on turbulence simulation. *J. Statist. Phys.* **121**, 823–841.